

An edited version of this paper was published by [AGU](#).

An eddy-permitting model of the Atlantic circulation: Evaluating open boundary conditions

Treguier, A. M.^{a,*}; Barnier, B.^b; De Miranda, A. P.^b; Molines, J. M.^b; Grima^c, N.; Imbard^d, M.; Madec, G.^a; Messenger, C.^e

^a Laboratoire de Physique des Océans, CNRS-Ifremer-UBO, Brest, France

^b Laboratoire des Ecoulements Géophysiques et Industriels, University of Grenoble, France

^c Institut du Développement et des Ressources en Informatique Scientifique, Orsay, France

^d Laboratoire d'Océanographie Dynamique et de Climatologie, CNRS-UMPC-IRD, Paris, France

^e Laboratoire d'Etude des Transferts en Hydrologie et Environnement, University of Grenoble, France

*: Corresponding author : treguier@ifremer.fr

Abstract:

As part of the French CLIPPER project, an eddy permitting model of the Atlantic circulation has been run for 22 years. The domain has open boundaries at Drake passage and at 30 °E, from Africa to Antarctica. The simulated mean circulation, as well as the eddy activity, is satisfactory for a 1/3° model resolution, and the meridional heat transport at 30 °S is within the range estimated from observations. We use the “mixed” open boundary algorithm of *Barnier et al.* [1998], which has both a radiation condition and a relaxation to climatology. The climatological boundary forcing strongly constrains the solution in the whole domain. The model heat balance adjusts through the surface (heat flux retroaction term) more than the open boundaries. The radiation phase velocities calculated within the algorithm are analyzed. This shows, quite surprisingly, that both the eastern and western boundaries have a similar behavior, regardless of the preferred directions for advection (mainly eastward) and wave propagation (mainly westward). Our results confirm that open boundary algorithms behave differently according to the dynamics of the region considered. The passive boundary condition that *Penduff et al.* [2000] applied successfully in the north eastern Atlantic does not work in the present South Atlantic model. We emphasize the need for a careful prescription of the climatology at the open boundary, for which a new approach based on synoptic sections is implemented. © 2001 American Geophysical Union

1. Introduction

Modeling the oceanic circulation is made difficult by the wide range of spatial scales from the Rossby radius of deformation (10 to 50 km) to the basin scales. Geostrophic eddies, narrow boundary currents, and flows through passages are important elements of the global circulation, and only models with high horizontal resolution can represent their effects. Given finite computer resources, there is always a trade-off between high resolution and global model coverage.

The CLIPPER modeling project is a French contribution to the World Ocean Circulation Experiment (WOCE). Our strategy is to concentrate computational resources on the Atlantic Ocean, which requires the prescription of artificial “open” boundary conditions at the edges of the model domain. CLIPPER builds on our previous experience with local area models of the South Atlantic [Barnier *et al.*, 1998; de Miranda *et al.*, 1999]. Model configurations with increasing spatial resolution (from 1° to $1/6^\circ$) have been implemented in the whole Atlantic domain from Antarctica to 70°N . We present here results of an eddy-permitting configuration of the CLIPPER model ($1/3^\circ$ at the equator), referred to as ATL3.

The choice of boundary conditions is extremely important for the circulation in the South Atlantic because of its geometry. It communicates with both the Pacific Ocean through Drake passage and with the Indian Ocean between Africa and Antarctica. Strong currents cross these boundaries: the inflowing Agulhas Current, with a transport of about 70 Sv [Beal and Bryden, 1997], and the Antarctic Circumpolar Current, with a transport at Drake passage of 130 to 140 Sv [Rintoul, 1991; Bryden and Pillsbury, 1977]. This is in sharp contrast with the North Atlantic Ocean, which has been modeled as a closed basin with some success: the Community Modeling Effort (CME) experiments [Bryan *et al.*, 1995], the Dynamics of North Atlantic Models (DYNAMO) experiments [Willebrand *et al.*, 2001], and recent high resolution models [Smith *et al.*, 2000; Paiva *et al.*, 1999].

The goal of the present paper is to analyze the role of the open boundaries in the ATL3 model solution. We expect it to depend, to some extent at least, on the numerical algorithm we have chosen. It would be desirable to test various algorithms and select the one which works the best, as, for example, Palma and Matano [1998] did for the barotropic case. However, even at eddy-permitting resolution, a realistic basin model is too costly to allow such a strategy. From previous experience we know that algorithms that work in an idealized case may give wrong results when the dynamics become more complex, with

stratification, bottom topography, and forcing [Barnier *et al.*, 1998; Marchesiello *et al.*, 2001]. The open boundary problem is mathematically ill-posed for the shallow water equations [Bennett and Kloeden, 1978] as well as for the primitive equations, which means that a “best” algorithm valid over a broad range of flow dynamics may not exist.

Given those constraints we have to choose a priori an algorithm and data to force the boundary. We use an algorithm that has been tested in a similar configuration [de Miranda *et al.*, 1999], and we propose an original method to calculate the boundary forcing. We then proceed with a thorough a posteriori evaluation of the open boundary behavior. This has never been documented in detail in a basin-scale model. The first question we address is the role of the open boundaries in the heat balance, as the model adjusts from its initial conditions. We then turn to the biggest unknown in the boundary forcing: the barotropic stream function. Can the model solution adjust at the boundary, as demonstrated by Penduff *et al.* [2000] in the case of an eastern Atlantic model? Or on the contrary, are the initial choices we make for the barotropic flow a strong constraint on the solution at all times? Finally, we study the radiative velocities at the boundaries to quantify the active or passive character of each boundary, and confirm our findings by a sensitivity experiment with fixed boundary conditions.

2. Model Description

Details about the ATL3 configuration are found in a report [CLIPPER Project Team, 1999b]; key parameters are presented in Table 1. We use the primitive equation code OPA8.1 developed at Laboratoire d’Océanographie Dynamique et de Climatologie (LODYC) [Madec *et al.*, 1998]. It is a second-order finite difference model with a rigid lid. The model configuration is similar to the “level” DYNAMO experiment [Willebrand *et al.*, 2001] except for the grid (“B” grid for LEVEL and “C” grid here) and the lateral boundary condition (we choose a free-slip boundary condition to make the flow less viscous over topographic slopes).

The horizontal grid is a Mercator isotropic grid with resolution $1/3^\circ$ at the equator. The grid has been locally deformed in the Strait of Gibraltar, retaining properties of orthogonality and continuity of the grid spacing. This allows a resolution of 10 km in the Strait of Gibraltar and the Alboran Sea. The vertical grid has 42 geopotential levels with a grid spacing of 12 m at the surface and 200 m below 1500 m. The bathymetry is calculated from Smith and Sandwell [1997] (details are found in Appendix A).

A horizontal biharmonic operator is used for lateral

Table 1

mixing of tracers and momentum, with a coefficient varying as the third power of the grid spacing, as in the DYNAMO models [Willebrand *et al.*, 2001]. The vertical mixing of momentum and tracers is calculated using a second-order closure model [Madec *et al.*, 1998]. In most of the ocean outside the surface mixed layer, the Richardson number is large enough so that the coefficient equals the constant background value (Table 1). In the case of static instability the vertical mixing coefficients are set to a very large value.

The model domain covers the Atlantic Ocean (Figure 4). Buffer zones are defined next to the closed boundaries in the Norwegian Sea, Baffin Bay, Weddell Sea and Alboran Sea. The buffer zones are defined as in DYNAMO [Willebrand *et al.*, 2001; CLIPPER Project Team, 1999b], with relaxation times ranging from 3 days to 100 days.

The model is initialized using the seasonal climatology of Reynaud *et al.* [1998]. The model integration starts in the Northern Hemisphere winter season (February 15). Seasonal values of temperature and salinity are interpolated linearly in time to serve as relaxation fields in the buffer zones. Note that for the Weddell Sea, Labrador Sea, and Baffin Bay, the annual mean was used because the amount of data was not sufficient to compute a reliable seasonal cycle.

The surface forcing fields are derived from the European Centre for Medium-Range Weather Forecasts (ECMWF) reanalysis ERA-15 averaged over the 15 years period from 1979 to 1993 [Garnier *et al.*, 2001]. The heat flux is formulated as suggested by Barnier *et al.* [1995], using their feedback coefficient for relaxation to the Reynolds sea surface temperature field. The evaporation minus precipitation flux is formulated as a pseudo salt flux, including river runoff. More details are found in Appendix A.

The model has been integrated for 22 years. Yearly averaged fields have been calculated from snapshots saved every 4 days.

3. Open Boundary Conditions

3.1. Algorithm

Two classes of open boundary conditions are used in ocean models, which are generally referred to as “active” or “passive”. Passive boundary conditions are used when the model solution is completely determined inside the domain of interest, and open boundaries are needed merely to allow the free radiation of disturbances to infinity. Such conditions, also called “radiative” boundary conditions, were first introduced by Orlandi [1976], and are relevant

in the case of hyperbolic equations. A recent review is found in the work by Palma and Matano [1998]. On the other hand, “active” boundary conditions are used when the boundary is supposed to force the interior solution. The latter conditions are naturally relevant to elliptic equations.

The boundary conditions used in CLIPPER are derived from those of the South Atlantic model developed for the Modélisation de l’Océan Atlantique (MOCA) project [Barnier *et al.*, 1998]. They are both active and passive and could therefore be defined as “mixed” (although Marchesiello *et al.* [2001] describes them as “adaptive”). “Mixed” or “adaptive” boundary conditions are intended to deal with complex, realistic flows where information may either flow out of the domain or into it. Furthermore, the inward or outward direction of the information flux is expected to vary in space and time according to the eddies and waves that develop in the model domain, and according to the external surface forcings.

The first part of the algorithm consists in calculating a phase velocity to determine whether perturbations tend to propagate toward, or away from, the boundary. Let us consider a model variable ϕ . The phase velocity ($C_{\phi x}, C_{\phi y}$) for the variable ϕ , in the directions normal and tangential to the boundary is

$$C_{\phi x} = \frac{-\phi_t}{(\phi_x^2 + \phi_y^2)} \phi_x \quad C_{\phi y} = \frac{-\phi_t}{(\phi_x^2 + \phi_y^2)} \phi_y. \quad (1)$$

Orlandi’s [1976] algorithm used only the normal velocity and set $\phi_y = 0$ in (1), while Raymond and Kuo [1984] advocated the use of both normal and tangential velocities. Following Barnier *et al.* [1998] we retain only the normal projection of the total velocity, $C_{\phi x}$, so we set $C_{\phi y} = 0$ (but unlike Orlandi we retain ϕ_y in the expression for $C_{\phi x}$). This approximation is described in detail by Marchesiello *et al.* [2001]. The discrete form of (1), described by Barnier *et al.* [1998], takes into account the two rows of grid points situated inside the domain next to the boundary, and the three previous time steps ($n, n-1$, and $n-2$). The same equation can then be discretized at the boundary at time steps n and $n+1$ in order to extrapolate the new boundary value ϕ^{n+1} .

In a “mixed” open boundary algorithm, the new boundary values are updated differently according to the sign of $C_{\phi x}$. There are two open boundaries in ATL3, at Drake passage and 30°E. Let us take the latter as an example:

$$\phi_t = -C_{\phi x} \phi_x + \frac{1}{\tau_o} (\phi_c - \phi) \quad (C_{\phi x} > 0), \quad (2)$$

$$\phi_t = \frac{1}{\tau_i} (\phi_c - \phi) \quad (C_{\phi x} < 0), \quad (3)$$

where ϕ_c is a climatological or observed estimate of ϕ at the boundary. Note that in (2), C_{ϕ_x} is bounded by the ratio $\delta x/\delta t$ for stability reasons. For our $1/3^\circ$ model at 50°S , $\delta x/\delta t = 10 \text{ m}\cdot\text{s}^{-1}$. When C_{ϕ_x} is eastward (outward propagation), the radiation condition (2) is used. When C_{ϕ_x} is westward (inward propagation), (3) is used with a strong relaxation to climatology ($\tau_i = 1$ day). The time derivative in (3) is calculated with a Euler time-stepping scheme. In that case, setting τ_i equal to the time step is equivalent to imposing the climatology for inflow conditions, a choice found to be numerically unstable for the barotropic mode in the energetic region of the Agulhas Current. The final value of 1 day thus appeared as a good compromise which guaranteed that the inflow conditions remain close to climatology while ensuring numerical stability.

Even in the outflow condition (2), a relaxation to climatology is maintained. The values of τ_o are indicated in Table 1 and will be discussed later.

The radiation scheme is used independently for the barotropic stream function (ψ), the baroclinic zonal velocity (u), and meridional velocity (v). The radiation velocity C_v is used for the temperature and salinity fields as well. Deciding how the radiation conditions should apply to the different variables of the model is quite arbitrary. It seems natural to treat separately the barotropic mode, which has different space scales and timescales. On the other hand, one may assume that a single radiation velocity could apply to the baroclinic fields. *Palma and Matano* [1998] report that using a radiation condition independently on all prognostic variables led to a numerical instability in the Princeton Ocean Model, while *Barnier et al.* [1998] did not experience the same problem with the Semi Spectral Primitive Equations (SPEM) model. *Stevens* [1990] developed open boundary conditions for the Geophysical Fluid Dynamics Laboratory (GFDL) primitive equation model. He calculated a radiation velocity for temperature, and obtained the velocities u and v at the boundary from geostrophy. This approach is difficult to implement in our model because it is discretized on a ‘‘C’’ grid (The GFDL model uses a ‘‘B’’ grid). Since u and v are not located at the same longitude, it was found necessary to calculate separate phase velocities C_u and C_v . On the other hand, v points are located at the same longitude as T and S which is why the phase velocity C_v was used for tracers as well. This procedure was found to give the best results in the MOCA model [*Barnier et al.*, 1998].

Finally, because some numerical instabilities occurred during the spin-up phase, the coefficient for biharmonic mixing of momentum was increased progressively by a factor of up to 8, over the eight grid points adjacent to the eastern boundary south of 40°S . No increase was neces-

sary near the western boundary, and no increase was performed in the Agulhas region north of 40°S because the solution did not present any anomaly there.

Our design for open boundaries differs significantly from *Stevens*’ [1991] implementation of the northern boundary in the Fine Resolution Antarctic Model (FRAM). In FRAM no radiation condition was applied on the barotropic stream function, and the tracers at the boundary were calculated using a more complete equation than (2). *Stevens*’ equation includes vertical diffusion and nonlinear advection. He did not show that those additional terms are important: *Stevens* [1990] only demonstrated the importance of the radiative term. In our model, preliminary tests have suggested that using a more complete equation does not make much difference, because the radiative phase velocities can be quite large. Therefore, in the prediction equation for a variable ϕ at the boundary, the $C_{\phi_x}\phi_x$ term tends to be the dominant one.

3.2. Providing Information at the Open Boundaries

The ‘‘climatology’’ constraint of the algorithm, ϕ_c in (2) and (3), requires a knowledge of the absolute velocity, temperature, and salinity at the boundary. Our rigid lid model also requires prescription of the transport around Antarctica. Lacking reliable information on the seasonal variability of this transport, we choose to impose a constant value of 140 Sv. Hydrographic data provide T , S , and baroclinic velocities (assuming geostrophy); the main problem is to find the barotropic component of the velocities along the boundaries. In previous South Atlantic models, both *Barnier et al.* [1998] and *Gan et al.* [1998] used simple analytical formulae for the barotropic stream function. In both cases the largest part of the barotropic transport was assumed to take place in the northern part of Drake passage. In the FRAM model [*Stevens*, 1991], the streamfunction at the northern open boundary was calculated from the monthly wind field using the Sverdrup relation. Such a procedure is not possible in the Antarctic Circumpolar Current at the latitude of Drake passage since there is no continental eastern boundary to integrate from.

Preliminary experiments with a low-resolution model have shown a large sensitivity to the value of the barotropic stream function at Drake passage [*Theret*, 1998]. This led us to propose a less arbitrary method to define the barotropic velocities. It is based on the assumption of ‘‘equivalent barotropic’’ dynamics, which is confirmed by models and observations in the Antarctic Circumpolar Current (ACC) [*Killworth*, 1992]. In this hypothesis the currents are in phase over the vertical, and an integration of the geostrophic shear assuming zero bottom velocity gives a good order of magnitude of the total transport.

Barotropic velocities estimated in this manner are presented in Figure 1 using either the *Reynaud et al.* [1998] climatology or the WOCE synoptic section of *Roether et al.* [1993]. The total transports are 82 and 112 Sv, respectively. Because of the spatial filtering used to construct the climatology, the ACC frontal system is completely smoothed out in the first solution (solid curve in Figure 1). We choose the synoptic section on the hypothesis that the frontal structure is important to force an eddy-resolving model. The final barotropic velocities are calculated by smoothing the profile of Figure 1 to remove the recirculations, and rescaling it to reach the imposed transport of 140 Sv (Figure 2).

The “barotropic equivalent” hypothesis is not valid at 30°E, however. An integration of the geostrophic shear from the I6 WOCE section [*Park and Charriaud*, 1997] gives a total transport of 325 Sv, very far from the 140 Sv that the model requires. We have nevertheless taken this calculation as a first guess for the barotropic stream function, because its meridional structure ensures that the barotropic and baroclinic expressions of the major fronts are consistent. We have performed linear adjustments to the stream function to impose inflows of 60 Sv in the Agulhas Current and 20 Sv in the Weddell gyre. A large eddy present in the data south of the Agulhas [*Park and Charriaud*, 1997] has been smoothed to avoid numerical problems at the boundary. The resulting absolute velocities profile is presented in Figure 3.

The transports of heat and salt associated with that climatology are presented in Table 2. Note that the “heat transport” is in fact a transport of potential temperature referenced to 0°C, and depends on the volume transport. To give an order of magnitude, with a mean temperature at the Drake passage section of 1.6°, the difference between the mass transport we prescribe (140 Sv) and Rintoul’s (130 Sv) induces a heat transport variation of 0.06 PW. We have calculated the model transports based on volume rather than mass, using a constant value of the reference density (1020 kg .m⁻³) and of the heat capacity (4 10⁶). Transports estimated with the true in situ density and heat capacity are larger by 1%.

Table 2 shows that our climatological heat transport at the western boundary is very similar to the best estimates from inverse models; this validates our “equivalent barotropic” hypothesis. On the other hand, the value we prescribe at the eastern boundary is 50% larger than inverse model estimates. Table 2 shows that the model adjusts to a smaller heat transport, by a mechanism that will be discussed in the next sections.

4. Global Description of the Circulation

Before considering the behavior of the open boundary algorithm, we need to provide an overview of the model solution. To do so, we present a vertically integrated picture (the sea surface height) and the zonally integrated circulation (meridional overturning stream function).

4.1. Horizontal Circulation

Figure 4 shows the mean sea surface height (SSH) averaged over the last 3 years. We compare it to previous z coordinate models with similar spatial resolution: the 1/3° DYNAMO “level” model, hereafter LEVEL [*Willebrand et al.*, 2001] and the 0.28° global model of *Maltrud et al.* [1998], hereafter POP5. In the North Atlantic the circulation shows interesting differences with LEVEL. A front associated with the Azores Current appears at 35°N: The dynamics of this current are linked with the outflow of Mediterranean water as in the DYNAMO isopycnic model [*Jia*, 2001]. The Mediterranean outflow is explicitly represented in ATL3, with a baroclinic exchange of 1 Sv in the Strait of Gibraltar, and a buffer zone in the Alboran Sea to force Mediterranean water characteristics. A previous experiment more similar to LEVEL, with closed Strait of Gibraltar, had produced (like in LEVEL) a very weak Azores Current. Note, however, that the representation of the Mediterranean outflow is not completely realistic in ATL3, since the outflow water was found to be too high in the water column (there is an excess of salt at 500-700 m and a deficit below 1000 m). This problem is being investigated.

The transport through the Florida Strait is more realistic in ATL3 (26 Sv) than in LEVEL (15 Sv). This transport has been shown to depend on the details of the topography, which is usually adjusted subjectively by modelers in the area. The overall strength of the subpolar gyre is similar to LEVEL, but details of the fronts differ. The North Atlantic Current east of the Grand Banks shows a wide latitudinal spreading, different both from the observed behavior (main front at 50°N) and LEVEL (main front at 45°N). Instantaneously, the flow often shows three main branches as in LEVEL and the 0.28° resolution experiment of *Smith et al.* [2000]. The frontal structure is less visible in the mean due to large fluctuations.

In the South Atlantic, the main features of the circulation are reproduced by the model. The ATL3 solution shows a southward meander south of 60°S downstream of Drake passage, which does not appear in POP5. This meander probably results from an interaction of the flow generated at the boundary with the local topography.

The Brazil-Malvinas confluence zone is too far south

Figure 4

in ATL3 (45°S), but has the same structure as in POP5: a zonally oriented front between two recirculation cells (with an associated transport larger than 50 Sv each). One would expect the time-mean flow to reflect the observed northward excursion of the Malvinas Current. This excursion is present in σ coordinate models, where it may be overestimated [Barnier *et al.*, 1998; de Miranda *et al.*, 1999; Gan *et al.*, 1998]. The fact that z coordinate models like POP or CLIPPER do not represent this feature correctly suggests the importance of topographic steering of the boundary currents, either locally in the confluence zone or upstream of it.

The behavior of the Agulhas retroflexion region (no figure shown) is very similar in ATL3 and POP5. De Miranda *et al.* [1999] had found that an open boundary at 30°E allowed the formation of Agulhas eddies in the MOCA 1/3° model. Eddy formation also occurs in ATL3 even though the climatology imposed at the boundary is constant (no seasonal variation). Agulhas eddies are shed very regularly (3.7 per year in POP5 and 3.4 per year in ATL3), and follow a very regular path. The sea surface height variability shows an elongated region of high variability oriented to the north west (very similar to Plate 7 of Maltrud *et al.* [1998]). In satellite observations the maximum of eddy activity is more concentrated in the Agulhas region, suggesting that the model Agulhas eddies are too stable as they drift. The eddy kinetic energy is underestimated by a factor of about 3 to 5 in the region, but it becomes quite realistic when the model resolution is increased, in the CLIPPER 1/6° model configuration. A detailed model-data comparison is under way; results of the 1/6° CLIPPER model will be presented elsewhere.

4.2. Meridional Overturning and Meridional Heat Transport

In the North Atlantic at 25°N, both the heat transport (0.85 PW, Figure 5a) and the strength of the meridional overturning cell (13 Sv, Figure 5b) are similar to those of LEVEL. Willebrand *et al.* [2001] argued that LEVEL underestimates the overturning because of the large mixing which takes place downstream of Denmark Strait and the Iceland-Scotland ridge, destroying the densest water masses that make up the lower branch of the thermohaline cell. We have verified that the same phenomenon occurs in ATL3.

The main difference between ATL3 and LEVEL is that the maximum overturning remains stronger in ATL3 in the equatorial and South Atlantic. At 11°S, the overturning is still 13 Sv in ATL3 but only 8 Sv in LEVEL. Accordingly, the heat transport at 11°S is stronger in ATL3 than in LEVEL, although it remains smaller than the esti-

mates of Speer *et al.* [1996] and MacDonald and Wunsch [1996] (Figure 5a). This difference is probably due to the different domain geometries. LEVEL has an open boundary at 20°S, with the barotropic stream function prescribed from the Sverdrup relation as given by Stevens [1991] and the baroclinic velocity calculated from the Levitus [1982] climatology. It is likely that the highly smoothed climatology does not represent correctly the western boundary contribution to the northward heat transport.

5. Boundary Contribution to the Heat Balance

Let us consider first, as a reference, the heat balance of a DYNAMO-like North Atlantic subdomain between 17°S and 70°N. The volume-averaged temperature has been calculated for two experiments: one North Atlantic experiment (NATL), with a closed boundary at 17°S and the same buffer zone as the DYNAMO Sigma and Isopycnic models, and the present Atlantic experiment (Figure 6). The model drift is quite small in NATL, lower than obtained in the North Atlantic model of Smith *et al.* [2000]. On the other hand, it is significantly larger in ATL3. Table 3 shows the adjustment of the various terms in the heat balance between year 2 and 12 of both experiments. The heat flux into the northern buffer zone is quite large in both cases (0.2 PW), and stays almost constant during the length of the experiment. The difference between ATL3 and NATL is a larger heat flux at 10°S, and a larger surface flux. The surface heat flux seen by the model is different from the ECMWF flux because of the retroaction term, proportional to the difference between the model sea surface temperature (SST) and the observed SST. The ECMWF 86-88 climatology of Barnier *et al.* [1995] that was used for DYNAMO had an unrealistic heat loss over the subtropical gyre [Willebrand *et al.*, 2001], which does not appear in the Comprehensive Ocean-Atmosphere Data Set (COADS) forcing [Paiva and Chassignet, 2001]. The climatology of the ECMWF reanalysis (years 79-93) is not very different from the 86-88 one, with a heat loss of 0.86 PW between 10°S and 70°N. As pointed out by Willebrand *et al.* [2001], the models cannot accommodate such a large and unrealistic heat loss. The model SST remains cooler than the observed SST over most of the subtropical gyre, generating a corrective retroaction term that compensates this loss and makes the model flux more realistic.

Table 3 shows which terms in the heat balance can explain the model adjustment (namely, the decrease of the heating trend from year 2 to 12). Clearly, the model adjusts by a modification of its surface heat flux, due to the

Figure 6

Table 3

decrease of the retroaction term with time.

Let us now consider the balance in the whole Atlantic domain. To emphasize the role of the open boundaries, the domain has been divided into a northern “closed” region north of 30°S , and an “open” region south of 30°S corresponding to the Antarctic Circumpolar Current. The zonal fluxes are calculated a few degrees away from the open boundary itself (66°W and 26°E). The model heat balance averaged over the last 3 years of the model run is pictured in Figure 7, and values for years 2 and 22 are found in Table 3. Note that the fluxes have been calculated by averaging the 4-day snapshots, which means that both the time-mean and eddy components are included. We have found, however, that the eddy component is always small (usually a few percent, occasionally up to 10% of the total flux). The residual of the balance is due to the contribution of the diffusive fluxes, which have not been calculated explicitly. They are generally much smaller than the leading order terms.

The model conserves volume and not mass, and the contribution from Bering Strait is not taken into account. This makes the salt balance (displayed in Table 3) difficult to compare with observations. Overall, the model salinity tends to increase, as does the temperature. Even after 22 years the heating trend north of 30°S is quite large (0.21 PW, Figure 7). This happens even though the heat flux at 30°S is compatible with estimates based on observations. The meridional fluxes at 30°S and 67°N are remarkably stable in time. The heating trend slows down from year 2 to 22 due to the surface heat flux adjustment, just like for the North Atlantic experiment (Table 3).

On the other hand, the southern region seems to equilibrate faster, and adjustment near the open boundaries plays a part. The decrease of heat input by the zonal boundaries by 0.18 PW and the decrease of the surface flux by 0.14 PW both contribute to the decrease of the warming trend between years 2 and 22. Note that the surface flux correction term is always negative in this southern region (the ECMWF fluxes produce a heat gain of 0.28 PW integrated south of 30°S).

The estimation of the heat and salt balances shows that the fluxes near the open boundaries are different from the prescribed climatological fluxes (Table 2) and that they vary during the model spin-up phase. Let us try to understand whether the open boundary conditions play a significant part in this behavior.

6. Are the Boundaries Active or Passive?

If the open boundary algorithm works as expected, the active or passive character of the boundaries depends on

the phase velocities calculated by (1). If outward propagation dominates, the boundary is passive and has little influence on the interior solution. If inward propagation is prevalent, the boundary actively forces the interior.

We anticipated an asymmetric behavior of the two open boundaries, due to the general eastward advection by the Antarctic Circumpolar Current. We chose a short timescale $\tau_o = 15$ days for outflow conditions at Drake passage, effectively forcing an “active” character of the western open boundary. On the other hand, we assumed the eastern boundary would be passive, so that perturbations generated inside the domain would tend to propagate through that boundary, advected by the mean current. We chose a very small relaxation coefficient τ_o^{-1} (Table 1) following *Barnier et al.* [1998] but we believe the solution would be essentially the same with $\tau_o^{-1} = 0$.

6.1. Barotropic Flow

Our expectation was that the radiation condition would allow an adjustment of the somewhat arbitrary initial barotropic stream function ψ to the interior solution. Quite to the contrary, we find that ψ remains very close to the climatology at all times at both boundaries. Figure 8 shows an instantaneous profile of the stream function at the eastern boundary, which is barely distinguishable from the climatological profile. Other instantaneous profiles chosen at random have the same property. Because the relaxation coefficient τ_o^{-1} is negligible, this can happen only if inward propagation happens frequently at the eastern boundary. This is indeed the case, as shown in Figure 9. Outward (inward) propagations, as defined by the sign of C_ψ in (1), exist about 50% of the time at all latitudes. The behavior of the western boundary is not qualitatively different.

This contrasts with the propagations that one observes in time-longitude plots. At 44°S (Figure 10), between the Agulhas return flow and the polar front, the mean velocities are weak, and westward propagation is dominant, certainly due to the β effect. At 52°S (Figure 11), in the vicinity of the polar front, the mean eastward velocity is large and eastward propagation (advection of the perturbations by the mean current) is dominant. The two different dynamical regimes have a very weak signature in the open boundary phase velocity (from Figure 9, the percentage of outward (eastward) propagation grows only from 45% to 55% between 44°S and 52°S). The time evolution of the phase velocities at those two latitudes shows that the model often shifts from outward to inward propagation and vice versa (Figure 12). Phase velocities tend to be weaker at 52°S than at 44°S : This suggests that they do not capture the physical signal of advection by the polar front revealed by the time-longitude plot (Figure 11). Nu-

Figure 8

Figure 9

Figure 10

Figure 11

Figure 12

merical noise may have a large impact on the calculation in regions where the mean flow is weak, and may be the cause of the large values of the phase velocity at 44°S.

On one hand, Figures 10 and 11 show that the open boundary algorithm works in the sense that no spurious instability appears at the boundary. On the other hand, the physics of the open boundary are different from the interior, and phase propagations seem to weaken before reaching the boundary.

The barotropic mode dynamics have a dual character in our model. Because of the rigid lid assumption, the equation for the barotropic stream function is elliptic at each time step. In some sense, the model behavior is consistent with this elliptic character of the problem: Boundary conditions need to be specified at all times. On the other hand, the barotropic stream function evolves in time, and the evolution equation allows for Rossby wave propagation as well as advection by mean currents, both processes which are more often thought of as hyperbolic problems. Our calculation of the barotropic phase velocity does not seem to handle correctly the complex dynamics. A similar behavior is found in the model of *de Miranda et al.* [1999] (de Miranda, personal communication, 1999).

Note that although the barotropic stream function does not depart from the climatology imposed at the boundaries, it does so a few grid points away from it (Figure 8). The departure is due to the inconsistency between the a priori boundary forcing and the interior solution. Such inconsistency is unavoidable given the complexity of the model and the uncertainties of the initial conditions and forcing fields. In the present solution the inconsistency is small enough that the solution remains well behaved at all times, although an increase of the biharmonic coefficient in the southern part of the eastern boundary has been necessary to achieve that (section 3).

6.2. Baroclinic Flow

The baroclinic velocity, temperature, and salinity present some variations from the climatology at the boundary. The modifications are important only near the surface, and in localized regions, for example, at the polar front and in the Agulhas region in the case of the eastern boundary. The localized modification of the Agulhas retroreflection flow around 37°S, where the surface velocity departs from climatology by 0.1 m.s^{-1} , contributes to the adjustment of the heat transport at 30°E: The imposed climatological heat flux is 1.45 PW, and the model flux right at the boundary is 1.29 PW. A larger adjustment occurs away from the boundary to reach 0.93 PW at 26°E (Table 2).

However, although the open boundary algorithm seems

to allow a little more variation from the climatology for the baroclinic variables, the baroclinic phase velocities are not easier to interpret than the barotropic ones. The percentage of outflow conditions, integrated over depth at each latitude for the meridional velocity v , is shown in Figure 13. Instantaneous sections reveal small scale structure both horizontally and vertically. The same is true for the phase velocity associated with tracers.

7. Fixed Open Boundary Conditions

The above analysis suggests that the radiation condition at the open boundaries is not an essential ingredient of the ATL3 solution. To test this hypothesis, the model was run for 3 years without the radiation condition. This means that the values of prognostic variables at the boundary are set to the climatological values at the beginning of the experiment and held fixed thereafter. This experiment is labeled ATL3F and started from year 12 of experiment ATL3. The currents and eddies in the two solutions do not differ much from each other. Plots of sea surface height or meridional overturning (not shown) are similar to their ATL3 counterparts.

The heat transport at the western boundary does not change from ATL3 to ATL3F, as could be expected since ATL3 had a strong relaxation to climatology there. The heat transport right at the eastern boundary varies by 10%. The estimation for year 15 of ATL3 is 1.03 PW, calculated at the grid point next to the boundary. It is 1.12 PW for ATL3F, getting closer to the climatological value (1.45 PW). However, the zonal heat transport away from the boundary (at 26°E) varies only by 1%.

Observations suggest that perturbations in the Agulhas Current influence the formation of Agulhas eddies. The time series in Figure 12 shows that the radiation condition at the boundary provides a high-frequency forcing. With fixed open boundary conditions this forcing is absent, and fewer or no eddies could result. To investigate this effect, we have drawn time series of the barotropic stream function in both experiments at 17.5°E, 38°S, a location at which the Agulhas eddy formation is the dominant signal (Figure 14). The eddy shedding gets out of phase between the two experiments, but the frequency of eddy formation is not very different.

The comparison of those two experiments shows that radiation is not essential, neither to preserve the numerical stability of the solution nor for the eddy statistics, at least for the short duration of this test (3 years). The two solutions are not identical though; the barotropic stream function is weakened in the South Atlantic subtropical gyre in ATL3F compared to ATL3, which causes a significant in-

Figure 13

Figure 14

crease of 0.6 PW in the heat transport at 30°S. The two solutions would certainly diverge over longer timescales.

Stevens [1991], *Palma and Matano* [1998], *Barnier et al.* [1998] and *Marchesiello et al.* [2001], testing “mixed” open boundary algorithms, concluded that they successfully prevent accumulation of energy and spurious wave reflections in the vicinity of the boundaries. Our results agree with theirs in that respect. We suspect, however, that in many applications of mixed boundary conditions in realistic eddy-permitting basin-scale models, the boundary values present very modest departures from the climatology.

8. Discussion

Using an Atlantic eddy-permitting model with two open boundaries, we have shown that the boundary forcing (e.g., the climatological values of temperature, salinity, and absolute velocity) strongly constrains the solution, even at locations where perturbations seem to propagate out of the domain.

Our experiments seem in contradiction with *Penduff et al.* [2000], even though both cases deal with similar space scales and timescales. *Penduff et al.* used a mixed boundary condition in their regional model of the north eastern Atlantic Ocean. The main difference with our case is that they did not prescribe a climatology for the barotropic stream function. When the radiation condition is into the domain, persistence is used instead of strong relaxation to climatology. *Penduff et al.* showed how their model successfully reconstructs a realistic barotropic stream function along 40°W, given a very crude linear initial condition. We tried to use *Penduff et al.*’s algorithm at our eastern boundary, but after a few months this condition produced strong unrealistic eddies in the Agulhas return flow, which turned out to be numerically unstable. This is in agreement with the discussion of *Penduff et al.*, who argued that it is necessary to provide information at an eastern boundary, because the adjustment of the barotropic response to the wind field is performed by westward propagating Rossby waves. The boundary of *Penduff et al.* is a western boundary, and it is situated close enough to the European coast where Rossby waves are generated. This is probably why the “self adapting” open boundary condition can work in their case. In our model it is quite possible that the self-adapting condition would work at Drake passage (our western boundary). However, unlike *Penduff et al.* we have a reasonable climatology of the barotropic stream function at Drake passage, because the flow is equivalent barotropic there. On the other hand, the barotropic stream function at 30°E is arbitrary, and we

would have preferred to be able to adjust it according to the interior solution. None of the algorithm variants we tried succeeded in doing that.

The determination of the phase velocity seems to be the weakest part of the open boundary algorithm. Phase velocities in our model look like random noise. Our intuition is that all the algorithms tested in idealized models [*Palma et Matano*, 1998] would behave similarly in a high-resolution basin-scale primitive equation model. We believe the basic problem is the fact that the radiation velocity is calculated using only two or three grid points at the boundary. In the presence of nonlinear advection, a large spectrum of dispersive waves, eddies, and wind forcing, one cannot expect such a calculation to capture the most energetic and physically meaningful propagative signal. Our time-longitude plots (Figures 10 and 11) suggest that more physical estimates of phase velocities are possible for the barotropic mode, perhaps by taking into account a larger area next to the boundary and more time steps. A decomposition into vertical modes and a method of characteristics applied to the different modes could also be considered. Developing and testing new algorithms is beyond the scope of this paper. We hope, however, that our results will encourage thorough testing of new algorithms in complex, realistic ocean models.

We emphasize again that the boundary forcing, more than the algorithm itself, plays the major part in the solution. We have tested in the present model an original forcing method, based on synoptic WOCE sections rather than a climatology. The data have been collected during the austral summer, which means that we have not been able to prescribe a seasonal cycle at the boundary. We do believe, however, that the benefit of having better defined fronts and more realistic heat and salt transports largely compensates for this drawback. Until higher-resolution climatologies with better resolved western boundary currents and fronts are available, we advocate the use of synoptic sections, with eventually some smoothing applied when large transient eddies are present. Care should be taken to ensure consistency between the barotropic and the baroclinic flows at the boundary. The fluxes of heat and salt should (if possible) be compatible with estimates based on observations.

Good results may also be achieved by using global high-resolution models to constrain the boundary. This possibility was examined by *Barnier et al.* [1996], but was not retained because the global models available at the time had an unrealistic transport at Drake passage. The situation may improve with a new generation of high-resolution global models.

Appendix A: Model Bathymetry and Surface Forcing

The model bathymetry is calculated from *Smith and Sandwell* [1997] $1/30^\circ$ gridded field by averaging all the data points in each model grid box. This procedure smooths out the subgrid scales. Hand editing is performed in key areas determined according to *Thompson* [1995]. We tried to ensure communication across the mid-Atlantic ridge (one grid point wide at least) at Meteor fracture zone, Rio de Janeiro fracture zone, Romanche fracture zone, and Vema fracture zone. The depths of the following straits were adjusted at a few grid points after close inspection: Florida Strait and the passage between Cuba and Hispaniola, Gibraltar, Faroe bank channel, Vema channel, and two passes across Walvis Ridge in the South Atlantic. The bathymetry is also modified next to the open boundaries so that there is no normal gradient of topography over three grid points.

The surface forcings are derived from daily values of the ECMWF reanalysis ERA-15, covering the period from 1979 to 1993 [*Garnier et al.*, 2001]. Each field is averaged for individual days and smoothed using a 10-day running average. This procedure is roughly equivalent to using monthly means, and it is not necessary to perform a special interpolation to preserve monthly mean values [*Killworth*, 1996]. Heat fluxes and evaporation minus precipitation fluxes are interpolated linearly onto the model grid. A bicubic interpolation is preferred for the wind stress components to avoid discontinuities in the wind stress curl. The atmospheric data are extrapolated from the ocean onto the land on their original grid before performing the interpolation, to avoid contamination of the oceanic domain by land grid points.

The heat flux is formulated as suggested by *Barnier et al.* [1995]:

$$Q = \lambda(T_o - T_m) + Q(T = T_o),$$

where Q is the total forcing heat flux, $Q(T = T_o)$ is the observed (ECMWF) net flux, T_o is the observed sea surface temperature [*Reynolds*, 1988] and T_m is the upper layer model temperature. This formula is obtained by linearizing a bulk formula around T_o . The feedback coefficient λ was calculated by *Barnier et al.* [1995] from ECMWF data between 1986 and 1988. It depends on space and time (12 monthly values).

The evaporation minus precipitation (e-p) fluxes are formulated as a pseudo salt flux. The flux includes the ECMWF e-p and river runoffs located at the mouth of 18 major rivers in the Atlantic [*Vörösmarty et al.*, [1996] (see Table A1). The river runoffs vary seasonally. The flux is

distributed over a number of grid points proportional to the river importance (from one grid point for the eight smallest rivers to 23 grid points for the Amazon). A relaxation to the seasonal climatological sea surface salinity is performed with the same feedback coefficient as for the SST.

Acknowledgments. The CLIPPER modeling project is supported by various French institutions: CNRS, IFREMER, EPSHOM, CNES and Meteo-France. The calculations have been performed on the T3E computer at IDRIS (Orsay).

References

- Barnier, B., L. Siefridt, and P. Marchesiello, Thermal forcing for a global ocean circulation model using a three-year climatology of ECMWF analyses, *J. Mar. Syst.*, 6, 363-380, 1995.
- Barnier, B., P. Marchesiello, and A. P. de Miranda, Modelling the ocean circulation in the South Atlantic: A strategy for dealing with open boundaries, in *The South Atlantic, present and past circulation*, Edited by G. Wefer et al., pp. 289-304, Springer-Verlag, New York, 1996.
- Barnier, B., P. Marchesiello, A. P. de Miranda, J.M. Molines, and M. Coulibaly, A sigma-coordinate primitive equation model for studying the circulation in the South Atlantic I, Model configuration with error estimates, *Deep Sea Res.*, 45, 543-572, 1998.
- Beal, L. M. and H. L. Bryden, Observations of an Agulhas Undercurrent. *Deep Sea Res.*, 44, 1715-1724, 1997.
- Bennett, A. F., and P. E. Kloeden, Boundary conditions for limited-area forecasts, *J. Atmos. Sci.*, 35, 990-996, 1978.
- Bryan, F. O., C. W. Böning, and W. R. Holland, On the mid-latitude circulation in a high-resolution model of the North Atlantic, *J. Phys. Oceanogr.*, 25, 289-305, 1995.
- Bryden, H.L., and R.D. Pillsbury, Variability of deep flow in the Drake passage from year-long measurement, *J. Phys. Oceanogr.*, 7, 803-810, 1977.
- CLIPPER Project Team, Scientific and technical report 1998, *LEGI Internal Rep. CLIPPER-R3-99*, 130 pp, Lab. des Ecoulements Geophys. et Ind., Grenoble, 1999.
- CLIPPER Project Team, $1/3^\circ$ Atlantic circulation model forced by the ECMWF climatology: preliminary results, *LPO Internal Rep. 99-04*, 126 pp, Lab. de Phy. des Oceans, Brest, 1999.
- de Miranda, A. P., B. Barnier, and W. K. Dewar, Mode waters and subduction rates in a high-resolution South Atlantic simulation, *J. Mar. Res.*, 57, 213-244, 1999.
- DYNAMO Group, DYNAMO: Dynamics of North Atlantic Models: Simulation and assimilation with high resolution models. *Ber. Inst. Meereskunde Christian-Albrechts-Univ.*, 294. 334 pp., Kiel, Germany, 1997.
- Gan, J., L. A. Mysak, and D. N. Straub, Simulation of the South Atlantic Ocean Circulation and its seasonal variability. *J. Geophys. Res.*, 103, 10,241-10,251, 1998.
- Garnier, E., B. Barnier, L. Siefridt, and K. Beranger, Investigating the 15-year air-sea flux climatology from the ECMWF re-analysis project as a surface boundary condition for ocean

- models. *Int. J. Climatol.*, 20, 1653-1673, 2001.
- Jia, Y.L., On the formation of an Azores Current due to Mediterranean Overflow in a modeling study of the North Atlantic. *J. Phys. Oceanogr.*, 30, 2342-2358, 2000.
- Killworth, P. D., An equivalent-barotropic mode in the fine resolution Antarctic model. *J. Phys. Oceanogr.*, 22, 1379-1387, 1992.
- Killworth, P. D., Time interpolation of forcing fields in ocean models, *J. Phys. Oceanogr.*, 26, 136-143, 1996.
- Levitus, S., Climatological Atlas of the World Ocean, *NOAA prof. Pap.* 13, 174 pp, 1982.
- Macdonald, A., and C. Wunsch, An estimate of global circulation and heat fluxes, *Nature*, 382, 436-439, 1996.
- Madec, G., P. Delecluse, M. Imbard, and C. Levy, OPA 8.1 general circulation model reference manual, Notes de l'IPSL, Univ. Pierre et Marie Curie, Paris, 91 pp, 1998.
- Maltrud, M.E., R. D. Smith., A. J. Semtner, and R. C. Malone, Global eddy-resolving ocean simulations driven by 1985-1995 atmospheric winds, *J. Geophys. Res.*, 103, 30,825-30,853, 1998.
- Marchesiello, P., J.C. Mc Williams, and A. Shchepetkin, Open boundary conditions for long-term integration of regional oceanic models, *Ocean Modell.*, 3, 1-20, 2001.
- Orlanski, I., A simple boundary condition for unbounded hyperbolic flow, *J. Comput. Phys.*, 21, 251-269, 1976.
- Paiva, A.M., J.T. Hargrove, E.P. Chassignet, R. Bleck, Turbulent behavior of a fine mesh (1/12°) numerical simulation of the North Atlantic. *J. Marine systems*, 21,307-320, 1999.
- Paiva, A.M., and E.P. Chassignet, The impact of surface flux parameterizations on the modeling of the North Atlantic Ocean, *J. Phys. Oceanog.*, in press, 2001.
- Palma, E.D., and R. P. Matano, On the implementation of passive boundary conditions for a general circulation model: The barotropic mode, *J. Geophys. Res.*, 103, 1319-1341, 1998.
- Park, Y. H. and E. Charriaud, Hydrography and baroclinic transport between Africa and Antarctica on WHP section I6, *Int. WOCE Newslett.*, no.29, 13-16, 1997.
- Penduff, T., B. Barnier and A. Colin de Verdiere, Self-adapting open boundaries for a regional model of the eastern North Atlantic, *J. Geophys. Res.*, 105, 11,279-11,297, 2000.
- Raymond, X.H., and H.L. Kuo, A radiation boundary condition for circulation models, *J. Hydraul. Eng.*, 111, 237-255, 1984.
- Reynaud, T., P. Legrand, H. Mercier and B. Barnier, A new analysis of hydrographic data in the Atlantic and its application to an inverse modeling study, *Int. WOCE Newslett.*, no.32, 29-31, 1998.
- Reynolds, R. W., A real-time global sea surface temperature analysis. *J. Clim.*, 1, 75-86, 1988.
- Rintoul, S., South Atlantic inter-basin exchange, *J. Geophys. Res.*, 96, 2675-2692, 1991.
- Roether, W., R. Schlitzer, A. Putzka, P. Beining, K. Bulsiewicz, G. Rohardt, and F. Delahoyde, A chlorofluoromethane and hydrographic section across Drake Passage: Deep water ventilation and meridional property transport, *J. Geophys. Res.*, 98, 14,423-14,435, 1993.
- Sloyan, B., The circulation of the Southern Ocean and the adjacent ocean basins determined by inverse methods, Ph.D. thesis, Univ. of Tasmania, Hobart, Tasmania, Australia, 1997.
- Smith, R. D., M. E. Maltrud, F. O. Bryan, and M. W. Hecht, Numerical simulation of the North Atlantic Ocean at 1/10°. *J. Phys. Oceanogr.*, 30, 1532-1561, 2000.
- Smith, W. H. F. and D. T. Sandwell, Global seafloor topography from satellite altimetry and ship depth soundings, *Science*, 277, 1956-1962, 1997.
- Speer, K.G., J. Holfort, T Reynaud, and G. Siedler, South Atlantic heat transport at 11°, in *The South Atlantic, Present and Past Circulation*, edited by G. Wefer et al., pp. 105-120, Springer-Verlag, New York, 1996.
- Stevens, D.P., On open boundary conditions for three-dimensional primitive equation ocean circulation models, *Geophys. Astrophys. Fluid Dyn.*, 51, 103-133, 1990.
- Stevens, D.P., The open boundary condition in the United Kingdom Fine-Resolution Antarctic Model, *J. Phys. Oceanogr.*, 21, 1494-1499, 1991.
- Theret, M.L., Etude des conditions aux limites au passage de Drake dans un modèle à basse résolution de l'Atlantique, projet de fin d'études, Ec. Nat. des Sci. et Tech. Avancées, Paris, 62 pp, 1998.
- Thompson, S. R., Sills of the global ocean: A compilation. *Ocean Modell.*, 109, 7-9, 1995.
- Vörösmarty, C.J., B. Fekete, and B.A. Tucker., River Discharge Database, Version 1.0, vol. 0 through 6, Tech. Doc. in Hydrol. Ser. UNESCO, Paris, 1996.
- Willebrand, J., B. Barnier, C. Boning, C. Dieterich, P. Hermann, P. D. Killworth, C. Le Provost, Y. Jia, J.M. Molines, and A. L. New, Circulation characteristics in three eddy-permitting models of the North Atlantic, *Prog. Oceanogr.*, 48, 123-161, 2001.
- B. Barnier, A. P. de Miranda and J. M. Molines, Laboratoire des Ecoulements Géophysiques et Industriels, Université de Grenoble, BP 53, 38041 Grenoble, France.
- N. Grima, IDRIS, BP506, 91403 Orsay, France.
- M. Imbard and G. Madec, LODYC, Université de Paris VI, 4 place Jussieu, 75252 PARIS Cedex 05, France.
- C. Messenger, LTHE, Université de Grenoble, BP 53, 38041 Grenoble, France.
- S. Michel, T. Reynaud and A. M. Treguier, Laboratoire de Physique des Océans, IFREMER, BP70, 29280 Plouzane, France.

Received April 18, 2000; revised December 8, 2000; accepted January 11, 2001.

¹Laboratoire de Physique des Océans, CNRS-Ifremer-UBO, Brest, France

²Laboratoire des Ecoulements Géophysiques et Industriels, University of Grenoble, France

³Institut du Développement et des Ressources en Informatique Scientifique, Orsay, France

⁴Laboratoire d'Océanographie Dynamique et de Climatologie, CNRS-UMPC-IRD, Paris, France

⁵Laboratoire d'Etude des Transferts en Hydrologie et Environnement, University of Grenoble, France

Table 1. Numerical Parameters for the ATL3 Experiment

Parameter	Symbol	Value
Horizontal resolution		
Equatorial (maximum)	δx	37 km
Southern (minimum)	δx	9.6 km
Grid points		387×649
Vertical resolution (42 grid points)	δz	12 to 200 m
Time step	δt	2400 s
Bottom friction (quadratic)	C_d	$1.3 \cdot 10^{-3}$
Vertical diffusivity		
Background	ν_v	$1 \cdot 10^{-5} \text{m}^2 \text{s}^{-1}$
Convective	ν_c	$1 \cdot \text{m}^2 \text{s}^{-1}$
Biharmonic friction (maximum)	ν_h	$2.5 \cdot 10^{11} \text{m}^4 \text{s}^{-1}$
<i>Relaxation timescales</i>		
Outflow conditions		
Eastern boundary	τ_o	1500 days
Western boundary	τ_o	15 days
Inflow conditions (all boundaries)	τ_i	1 day

Table 2. Transports at the Open Boundaries^a

Boundary	Rintoul [1991]	Sloyan [1997]	ATL3 CLIM	ATL3 Model
Mass transport, Sv	130	134	140	140
Heat transport, PW				
Drake passage	1.3	1.3	1.46	1.44
Eastern boundary	1.2	1.	1.45	0.93
Salt transport, $10^{12}\text{kg}\cdot\text{s}^{-1}$				
Drake passage		4.73	4.92	4.92
Eastern boundary		4.74	4.92	4.92

^a The transports indicated are not calculated at the same locations. The “Eastern boundary” values of Rintoul and Sloyan are calculated with the AJAX2 section (along 0°E and up to the tip of Africa). Our ATL3 “climatology” (CLIM) is estimated at 30°E , using the section of *Park and Charriaud* [1997]. The ATL3 model values are calculated from the interior solution at 26°E (see text). For the western boundary, Rintoul used a section from 1975 in Drake passage, and Sloyan used the section of *Roether et al.* [1993], the same as the ATL3 climatology. The ATL3 model transports are estimated at 66°W .

Table 3. Heat and Salt Balances in Subdomains of the Model ^a

	South Flux ^b	North Flux ^c	Zonal Flux	Surface Flux	Heat Content Trend
<i>“DYNAMO” Domain for NATL and ATL3 Experiments: Heat Balance for Years 2 and 12</i>					
NATL	0.37 — 0.29	-0.18 — -0.19	0	0.22 — -0.02	0.4 — 0.08
ATL3	0.45 — 0.38	-0.19 — -0.21	0	0.35 — 0.05	0.58 — 0.19
<i>ATL3 Experiment: Heat Balance for Model Years 2 and 22</i>					
North	0.32 — 0.33	-0.19 — -0.22	0	0.5 — 0.15	0.58 — 0.23
South	-0.01 — -0.04	-0.32 — -0.33	0.69 — 0.51	0.09 — -0.05	-0.45 — 0.08
<i>ATL3 Experiment: Salt Balance ($10^6\text{kg}\cdot\text{s}^{-1}$) for Model Years 3 and 22</i>					
North	-4.7 — -2.9	-2.3 — -2.7	0	15.9 — 12.2	8.9 — 6.7
South	0.4 — 0.2	4.7 — 2.9	-1.4 — 0.4	0.5 — -1.3	3.7 — 2.

^aTwo values are indicated for each term, corresponding to different years. For the DYNAMO domain (10°S - 67°N) an experiment with closed boundary at 17°S (NATL) is compared with ATL3. Heat and salt balances are presented for ATL3 in the northern (30°S - 67°N) and southern (72°S - 30°S) parts of the domain. A positive flux indicates an input of heat (or salt) into the region. The zonal flux is the difference of fluxes at 66°W and at 26°E .

^bSouth flux is at at 10°S for the DYNAMO domain, 30°S for the “North” part of ATL3, and 72°S for the “South” part of ATL3.

^cNorth flux is at at 67°N for the DYNAMO domain, 70°N for the “North” part of ATL3, and 30°S for the “South” part of ATL3.

Table A1. Annual Mean Water Flux Into the Atlantic From 18 of the Most Important Rivers^a

River	Latitude	Longitude	Flux
Magdalena	11°	-75°	6,992
Atrato	8°	-77°	2,274
Orinoco	8°	-61°	28,856
Cuyuni, Essequibo	7°	-58°	3,569
Corantjn	6°	-57°	1090
Marowijne	6°	-54°	1889
Amazon	0°	-50°	166,953
Tocantins	-1°	-49°	12,092
Sao Francisco	-11°	-37°	2,635
Rio de la Plata	-34°	-58°	22,738
Rhine	52°	4°	2,278
Volta	6°	1°	1,123
Sanaga	4°	10°	2,007
Ogouee	-1°	9°	4,689
Congo	-6°	12°	41,128
St. Laurent	49°	-68°	12,270
Churchill	54°	-57°	1,863
Mississippi	29°	-89°	17,701

^am³.s⁻¹, UNESCO Data [Vörösmarty *et al.* 1996]

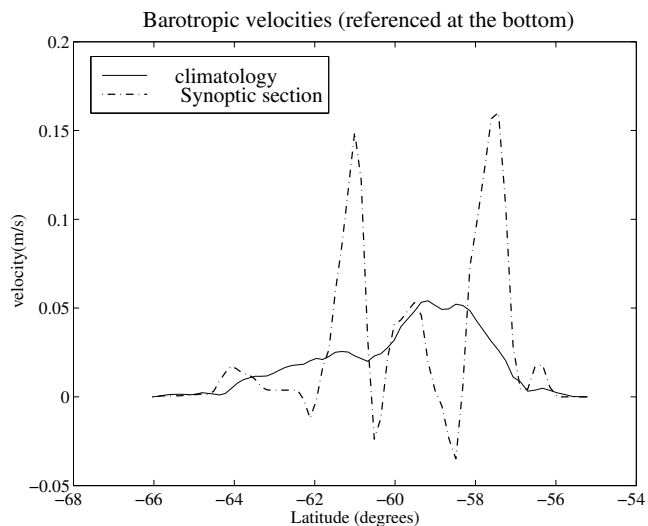


Figure 1. Barotropic velocity across Drake passage (geostrophy referenced to the bottom) with Reynaud's climatology and the WOCE section [Roether *et al*, 1993].

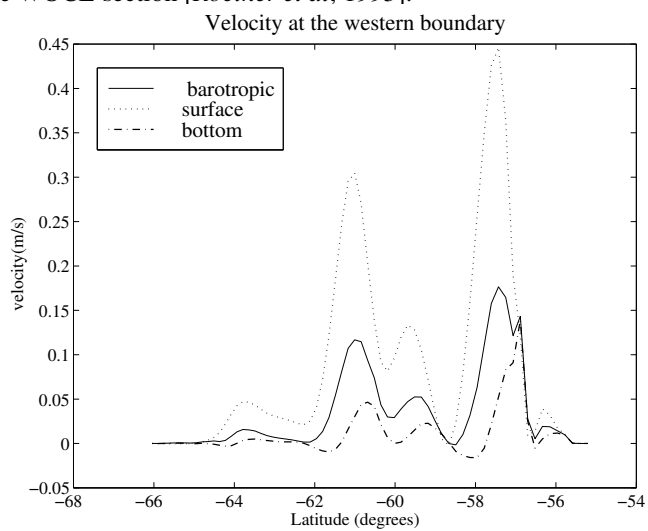


Figure 2. Absolute velocities at the western open boundary for the CLIPPER model.

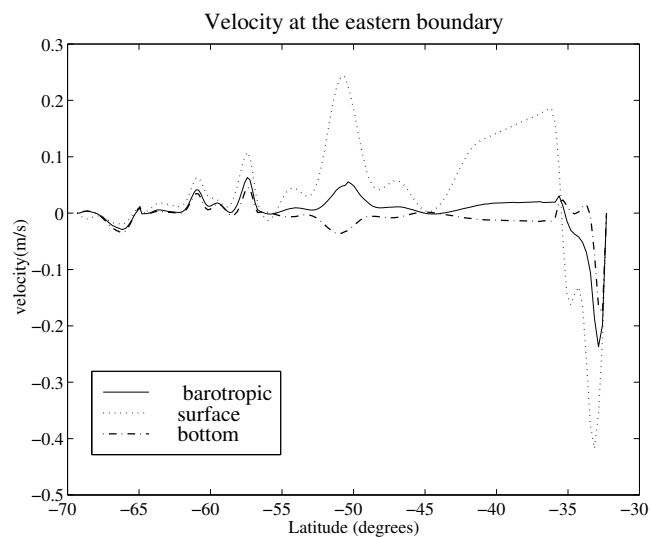


Figure 3. Absolute velocities at the eastern boundary for the CLIPPER model, derived from the WOCE I6 section.

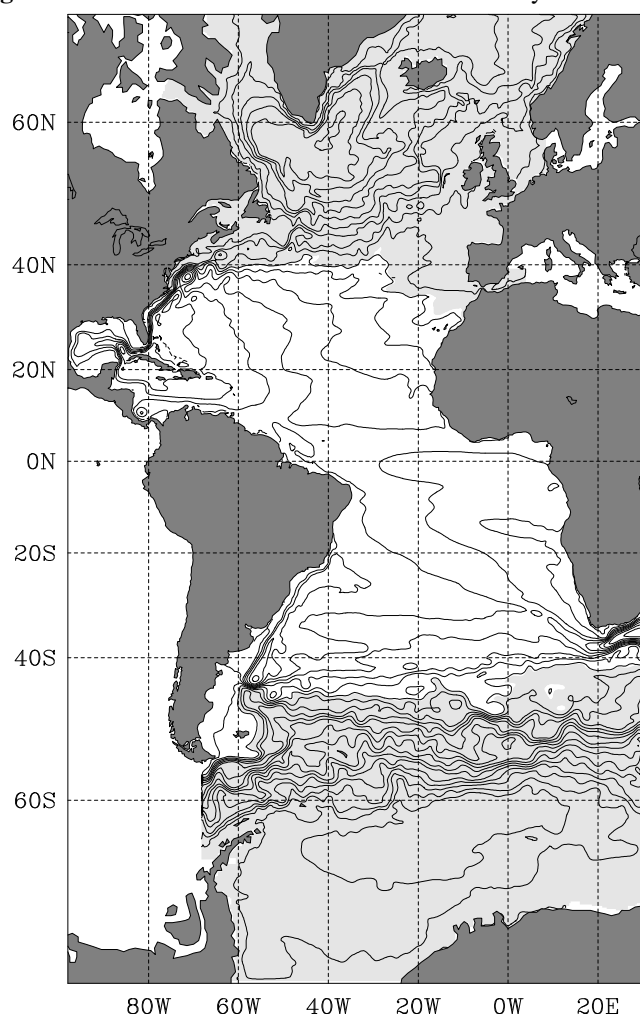


Figure 4. Sea surface height (SSH) averaged over the last three model years. Contour interval is 0.1 m. Negative values are shaded. The mean level over the model domain is taken to be zero

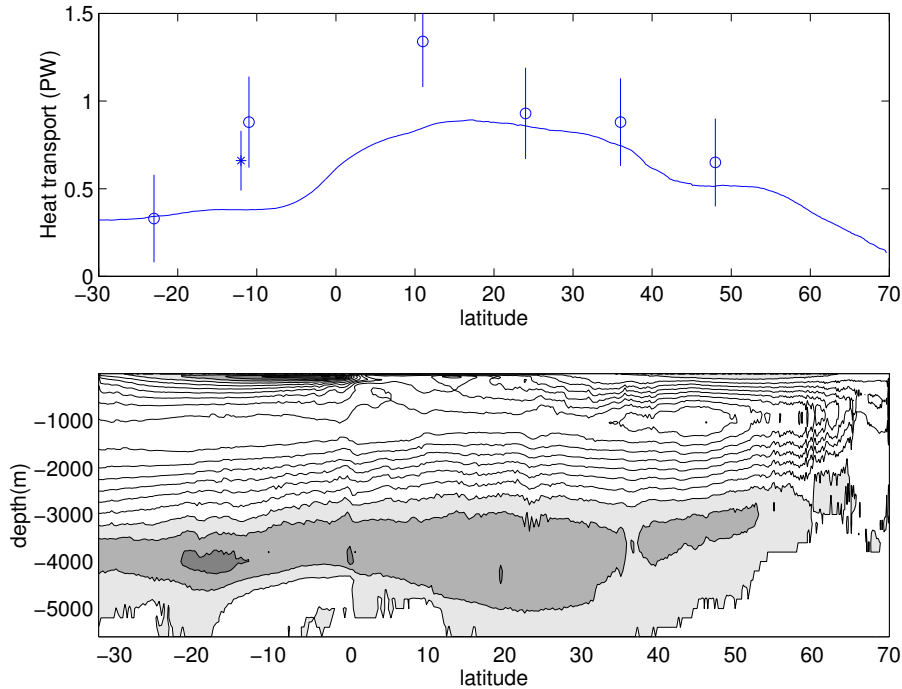


Figure 5. (a) Meridional heat transport averaged over the last three model years. Circles are estimates from *MacDonald and Wunsch* [1996]. The star is the estimate from *Speer et al.* [1996], shifted by 1° south to avoid overlap. (b) Meridional overturning stream function averaged over the last three model years. Contour interval is 2 Sv. Negative values are shaded.

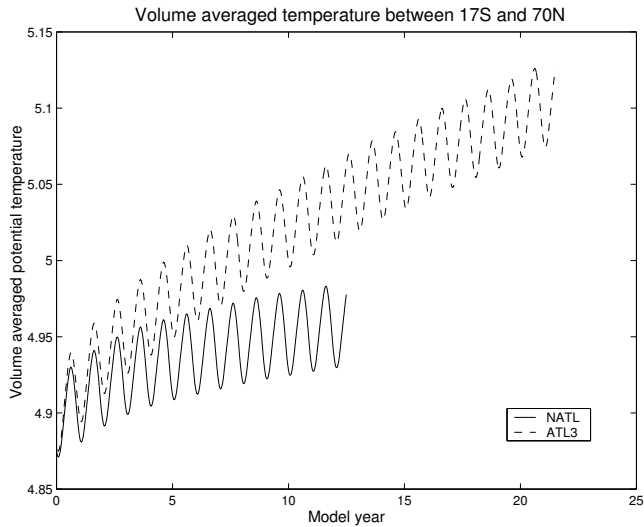


Figure 6. Time series of volume-integrated temperature north of 17° S in two experiments, with North Atlantic (NATL) and Atlantic domain (ATL3).

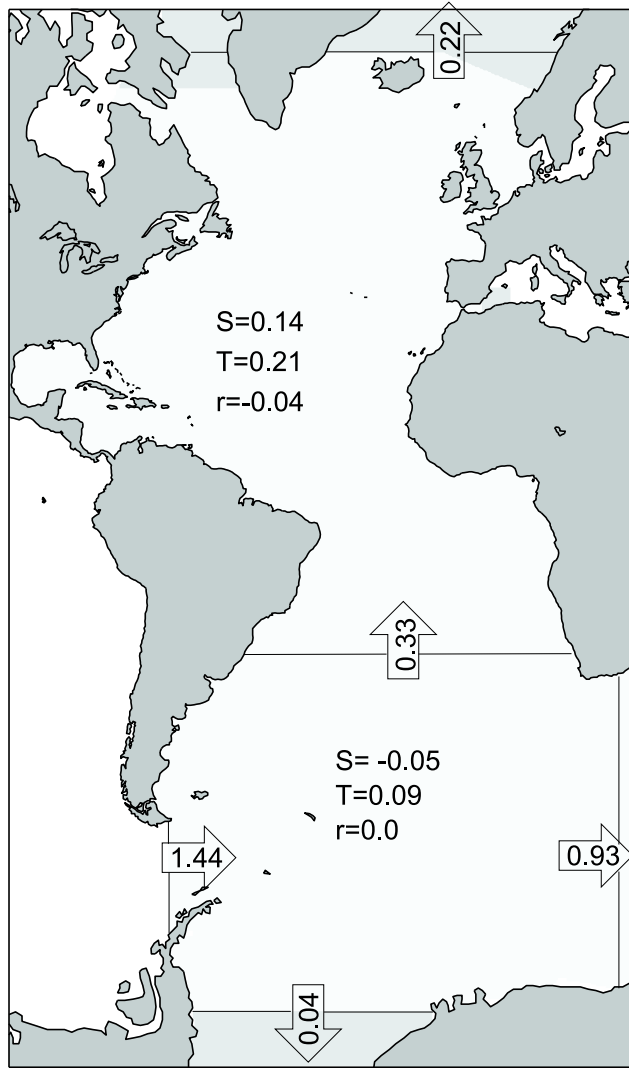


Figure 7. Heat balance of the model north and south of 30°S (Pw). Fluxes are averaged over the last three years of the experiment. Advective fluxes are indicated by arrows. For the zonal fluxes, temperature is referenced at 0°C . Only the difference between the Drake passage flux and the flux at 26°E is independent of the reference temperature. S is the surface flux, T is the trend (positive for heating), and r is the residual which is due to diffusive terms.

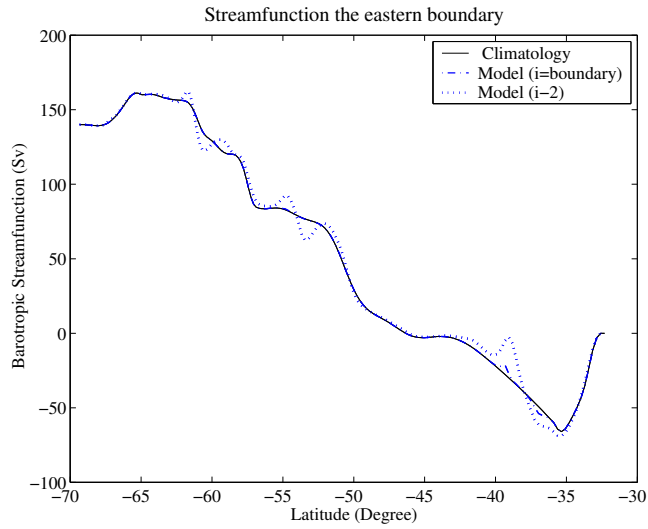


Figure 8. Profiles of barotropic stream function at the eastern boundary (Sv). The solid line is the climatology derived from the WOCE I6 section (see section 2). The dashed line is an instantaneous profile at the boundary, the dotted line an instantaneous profile two grid points away from the boundary.

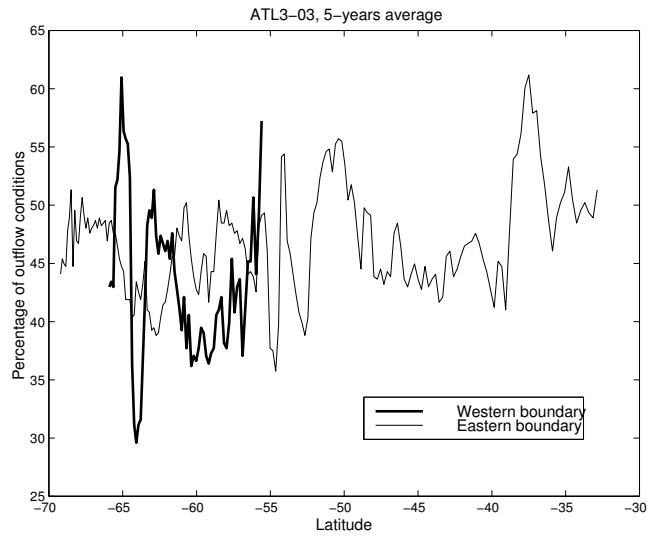


Figure 9. Percentage of outgoing phase velocities for the barotropic stream function, calculated over the last five years of the experiment, as a function of latitude along the open boundaries.

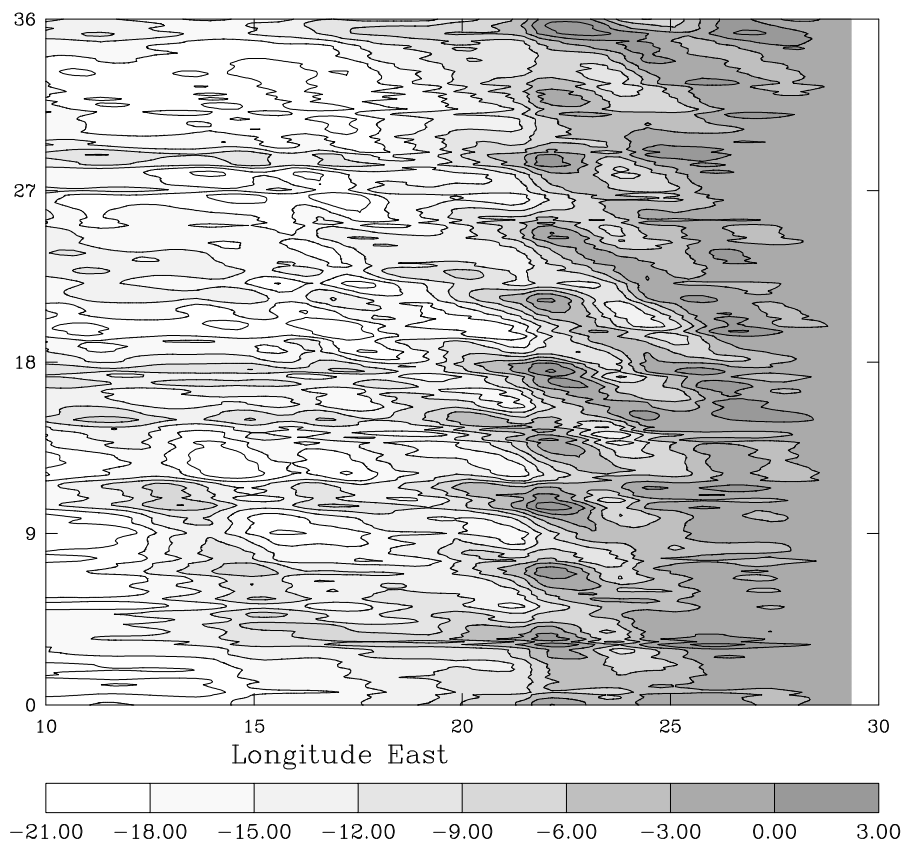


Figure 10. Time-longitude plot of the barotropic stream function at 44°S. Times are indicated in months.

Figure 11. Time-longitude plot of the barotropic stream function at 52°S. Times are indicated in months.

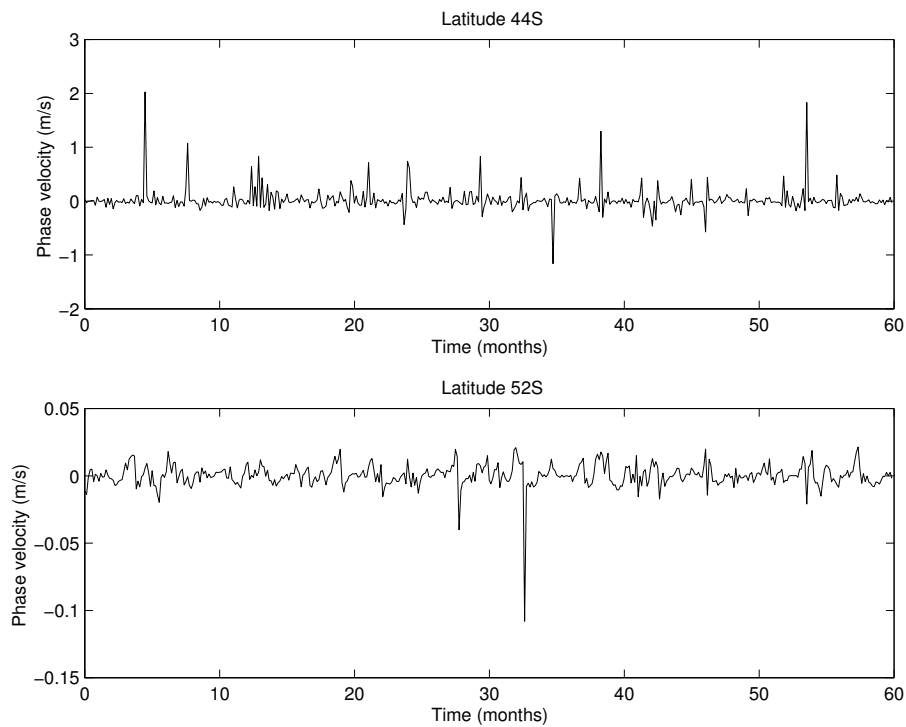


Figure 12. Phase velocities for the barotropic stream function, at 44°S and 52°S , over five years of the experiment.

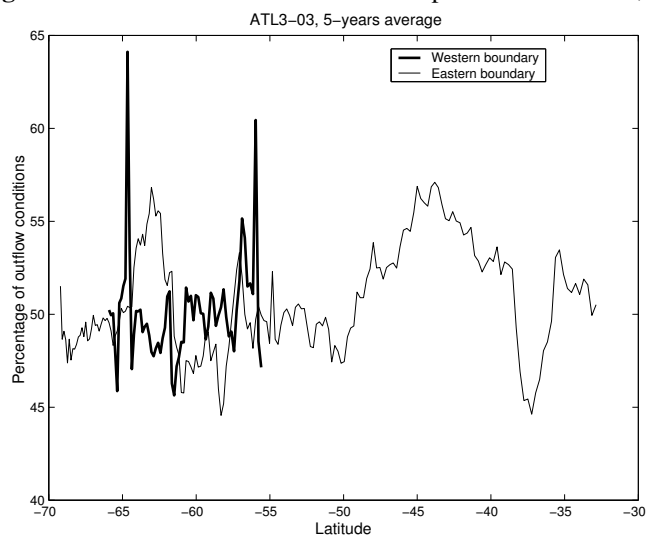


Figure 13. Percentage of outgoing phase velocities for the baroclinic meridional velocity v , averaged over depth and over the last five years of the experiment, as a function of latitude along the open boundaries.

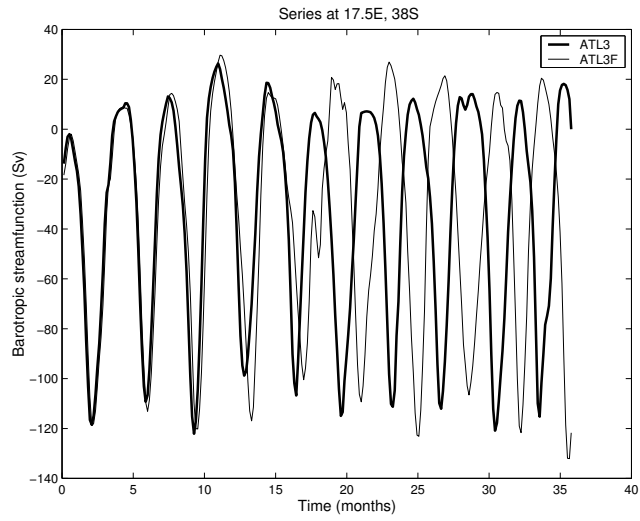


Figure 14. Time series of the barotropic stream function at 17.5°E, 38°S for the two experiments ATL3 and ATL3-F.